Generation of nanoplastics during the photoageing of low-density polyethylene

Carmen Sorasan, Carlos Edo, Miguel González-Pleiter, Francisca Fernández-Piñas, Francisco Leganés, Antonio Rodríguez, Roberto Rosal. Generation of nanoplastics during the photoageing of low-density polyethylene, Environmental Pollution, 289, 117919, 2021 https://doi.org/10.1016/j.envpol.2021.117919.

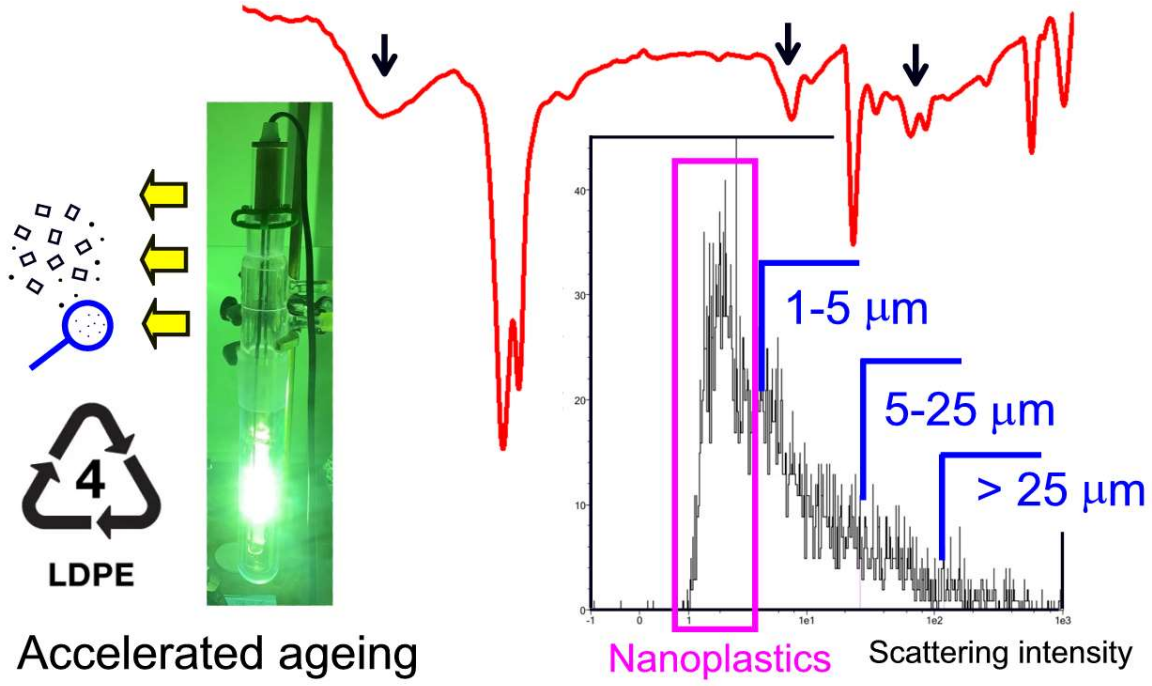

Generation of nanoplastics during the photoageing of low-density polyethylene

Carmen Sorasan[1], Carlos Edo[1], Miguel González-Pleiter[2], Francisca Fernández-Piñas[2], Francisco Leganés[2], Antonio Rodríguez[1], Roberto Rosal[1,*]

1 Department of Analytical Chemistry, Physical Chemistry and Chemical Engineering, University of Alcalá, Alcalá de Henares, E-28871 Madrid, Spain

2 Department of Biology, Faculty of Sciences, Universidad Autónoma de Madrid, Cantoblanco, E-28049 Madrid, Spain

* Corresponding author: roberto.rosal@uah.es

Abstract

In this work, we studied the hydrolytic and photochemical degradation of three low-density polyethylene (LDPE) materials, within the size range of microplastics (MP). The MPs were exposed to mechanical agitation and UV irradiation equivalent to one year of solar UVB + UVA in a stirred photoreactor. Flow cytometry was used to track the formation of small (1-25 μm) MPs by applying Mie's theory to derive the size of MP particles from scattering intensity readings. The calculation was based on a calibration with polystyrene (PS) beads. The results showed that the generation of 1-5 μm MPs reached 10^4-10^5 MPs in the 1-25 μm range per gram of LDPE. ATR-FTIR and micro-FTIR measurements evidenced the formation of oxygenated moieties, namely hydroxyl, carbonyl, and carbon-oxygen bonds, which increased with irradiation time. We also found evidence of the production of a high number of nanoplastics (< 1 μm, NPs). The Dynamic Light Scattering size of secondary NPs was in the hundreds of nm range and might represent up to 10^{10} NPs per gram of LDPE. Our results allowed the unambiguous spectroscopic assessment of the generation of NPs from LDPE under conditions simulating environmental exposure to UV irradiation and used flow cytometry for the first-time to track the formation of secondary MPs.

Keywords: Microplastics; Nanoplastics; Ageing; Flow cytometry; Ultraviolet irradiation

1. Introduction

Plastics are part of our lives since the middle of the last century. The worldwide plastic production in 2019 amounted to 368 million tonnes and the main end-use markets for plastics were packaging and building & construction representing 39.6 % and 20.4 % respectively of the plastic demand in the European Union (EU28 plus Norway and Switzerland) according to PlasticsEurope (PlasticsEurope, 2020). Their versatility, lightness, resistance, and low cost made them unique for the production of a huge variety of goods (Thompson et al., 2009). However, and despite of the efforts made to decarbonize plastic production, most plastics are produced from fossil sources and a circular economy of plastics is still far. The sector is expected to account for one fifth of the total oil consumption by 2050, representing 15 % of the global annual carbon budget (WEF, 2016). In Europe, only 29.1 million tonnes post-consumer plastic waste was collected in 2018, 57.4 % of the total plastic demand, and from that amount, still 7.2 million tonnes were sent to landfill. The plastic waste that ends up disseminated in the environment is difficult to estimate because of the complexity of trade flows along the life cycle of plastics (Barrowclough et al., 2020).

When dispersed into the environment, plastics undergo ageing and transformation processes due to biotic and abiotic processes. Abiotic degradation mechanisms are the consequence of physical factors leading to cracking and fragmentation and chemical changes associated to the leaking of stabilizers and bond cleavage due to hydrolysis, oxidation, or photochemical reactions (Chamas et al., 2020). Biotic transformations are the consequence of the action of microorganisms able to use synthetic polymers as carbon source (Ru et al., 2020). The main parameter governing the environmental fate of plastics is particle size. Plastics are defined as microplastics (MPs) if their largest dimension is smaller than 5 mm (GESAMP, 2019). This boundary is clearly arbitrary and even inconsistent with the prefix "micro". However, it has been widely accepted because of the need of preserving the existing body of information on the occurrence and fate of MPs in many studies published with the 5 mm cut-off (GESAMP, 2015, 2016). The lower size limit of MPs is generally taken as 1 μm below which, the particles are referred to as nanoplastics (NPs) if they display colloidal behaviour and come from the degradation of larger plastics (Gigault et al., 2018). Ageing processes lead to the fragmentation of plastic materials into smaller particles generating the so-called secondary MPs, as opposed to some plastics specifically produced in small sizes, which are referred to as primary MPs (Koelmans et al., 2017). There are few experimental studies on the alteration of polymers in natural

environments. Julienne et al. studied the artificial photodegradation of low-density polyethylene (LDPE) films and found that fragmentation was not correlated with the oxidation level, hydrolytic reactions being the main driver for cracking propagation (Julienne et al., 2019). The fragmentation of high-density polyethylene (HDPE) was studied by Kalogerakis et al. who found higher fragmentation rates on beach sand than in seawater, which was attributed to the combination of higher temperature, ultraviolet radiation, and mechanical stress due to sand abrasion (Kalogerakis et al., 2017). The weathering of plastics is usually addressed by spectroscopic techniques that identify the fingerprint of the typical moieties that appear upon hydrolysis and (photo)oxidation like hydroxyl, carbonyl, and carbon-oxygen groups. Fourier Transform Infrared (FTIR) or Raman spectroscopy have been used to identify the chemical changes produced during plastic ageing. Brandon et al. studied the changes in hydroxyl and carbon-oxygen bonds and correlated them with the time the plastics were exposed to degradation (Brandon et al., 2016). During the photodegradation of low-density polyethylene (LDPE), Hiejima et al. used Raman spectroscopy to assess an increase in crystallinity due to changes in the amorphous phase that accompanied the shrinkage and cracking of specimens (Hiejima et al., 2018).

The degradation of plastic polymers is known to produce low molecular weight fragments due to chain scission, including monomers and short-chain oligomers that would be classified as NPs, if their larger dimension is below 1 μm (Gewert et al., 2015). The occurrence and impact of NPs in natural environments have been largely discussed, but the methodological difficulties associated to their sampling make it difficult to draw conclusions on the real risk posed by NPs. Gigault et al. provided the first data indicating that PE could be source of NPs due to the effect of UV irradiation (Gigault et al., 2016). The same group studied the presence of NPs in soil by combining separation by asymmetric flow-field flow fractionation with pyrolysis coupled to gas chromatography/mass spectrometry to demonstrate the presence of NPs from several polymers in soil (Wahl et al., 2021). The presence of NPs from the fragmentation of the microbeads used in cosmetics has also been recently assessed (Hernandez et al., 2017). Although still very incomplete, the available data confirm that NPs are part of the anthropogenic plastic litter discharged to the environment or produced during the degradation of larger particles in environmental compartments. Compared to their non-polar larger counterparts, NPs are expected to be relatively polar and more prone to interact with the biota. The toxic effect of NPs on different organisms has been reported elsewhere (Gonçalves and Bebianno, 2021; González-Pleiter et al., 2019). The higher mobility of colloidal NPs facilitates their migration through porous media and makes it possible their uptake by plants and even their internalization in tissues if they are small enough to cross epithelial barriers. Plastic leachates also contain the additives included in the formulation of commercial goods, some of which are a source of toxicity that can spread through the trophic chains (Larue et al., 2021). Finally, NPs, more than MPs due to their higher specific surface, may interact with co-contaminants like heavy metals, emerging pollutants, polycyclic aromatic hydrocarbons, and other nanoparticles, among others. Such pollutants may adsorb onto or become transformed upon interaction with NPs influencing the toxicity of their mixtures (Bhagat et al., 2021).

In this work, we studied the degradation of three LDPE materials when exposed in aqueous media to the UV radiation equivalent to one year of solar irradiance combined with mechanical agitation. The irradiation was applied using a mercury lamp covering the solar wavelength with UVA+UVB irradiance (280 to 400 nm) of 1060 W m^{-2}. We used flow cytometry to quantify the small MPs (1-25 μm) formed during the degradation of MP pellets. Besides, we obtained direct evidence for the generation of NPs during the ageing of PE materials.

2. Experimental section

2.1. Materials

The PE (CAS 9002-88-4) materials used for this research were: (1) LDPE 5 mm pellets, injection moulding grade, ET316305, supplied by Goodfellow (Coraopolis, USA); (2) laboratory LDPE flasks, manually cut into small pieces of 4-5 mm; and (3) recycled LDPE pellets (5 x 2 mm) produced from residual greenhouse film kindly supplied by Green World Compounding (Alhama de Murcia, Spain). The reason for choosing three materials was to cover all the lifecycle of LDPE, from virgin pellets to recycled LDPE coming through plastic from commercial goods. Chemical differences are expected in the presence of different additives in commercial and recycled pellets, supposedly absent in virgin pellets, marketed as additive-free. In what follows these three LDPE microplastics are referred to as LDPE-1, LDPE-2, and LDPE-3 respectively. The average weight of pellets was 0.0257 g for LDPE-1, 0.0240 g for LDPE-1 and 0.0378 for LDPE-3. Prior to the experiments, MP pellets and fragments were washed twice with HPLC grade methanol (CAS 67-56-1), and with ultrapure water (Milli-Q Q-POD® Ultrapure Water System), after which they were dried, their weight recorded, and some specimens reserved for analyses.

2.2. Experimental procedure

The irradiation was provided by a 150 W medium-pressure mercury lamp (Novalight TQ150) emitting in the 297-579 nm range. The emission spectrum is given in Fig. S1, Supplementary Material, SM. The irradiation experiments were conducted to mimic one year of solar radiation. The equivalence was calculated

using the NASA Surface meteorology and Solar Energy database recording the monthly averaged insolation for the latitude of Madrid, which is in average 4.4 kWh m^{-2} day^{-1} (183 W m^{-2}). The average irradiance in middle point of the liquid exposed was 1060 W m^{-2} (UVB + UVA or 280-400 nm). Considering 5 % of the solar irradiance corresponds to UVA + UVB, 1 year was equivalent to approximately 3 days or 72 h of irradiation in our device. The irradiance was measured using a Modular Spectrometer System UV-Vis (StellarNet) equipped with SpectraWiz Spectrometer OS v5.33 software.

The experiments were performed in a 1 L photochemical reactor thermostated at 24 °C and magnetically stirred at 700 min^{-1} to provide homogenous exposure. The reactor was filled with 500 mL ultrapure water (Milli-Q resistivity > 10 MΩ cm, filtered 0.22 μm) and loaded with 10 % (w/v) MPs. Non-irradiated runs provided the fragmentation pattern due to hydrolysis and mechanical stress, whereas irradiation gave combined information on hydrolysis, mechanical stress, and photooxidative degradation. Additional runs were performed in the darkness and in the absence of any agitation, to clarify the role of mechanical stress in the release of secondary particles. All runs were performed at least twice, and all analyses were replicated. During the runs, samples were taken every 24 h to assess the physicochemical properties of MPs, and the generation of secondary fragments consisting of smaller MPs and NPs. The liquid was sampled by taking 25 mL aliquots from the central part of the reactor without stopping the stirrer. Additionally, five pellet particles were removed to perform spectroscopic, imaging, and mechanical studies. The samples were identified with LDPE-Plastic type-[Time]-Irradiation, where "Plastic type" was 1 (Goodfellow pellet), 2 (commercial flasks) or 3 (pellets from recycled greenhouse film); "time" corresponds to the sample (0 or initial and taken after 24, 48 and 72 h); and "irradiation" differentiates between irradiated (I) and non-irradiated (NI) runs. Non-irradiated/non-stirred runs were denoted as NI/NS. Aliquots of the samples were filtered using 1 μm pore size Puradisc 25 TF filters to separate submicron particles and dissolved material from larger MPs. Other aliquots were reserved for analyses as indicated below. A part of the final reaction mixture was filtered using 25 μm stainless steel mesh in order to obtain samples from the secondary MPs > 25 μm generated from the original MPs. Additionally, irradiated runs were performed in two ways. In one set of runs, the pellets were put in water stirred and irradiated for the prescribed time (72 h, Procedure I), while in another set, the liquid obtained at the end of stirred and non-irradiated runs was further irradiated under stirring for another 72 h after withdrawing the pellets, indicated below as Procedure II.

2.3. Analytical procedures

Infrared spectra were acquired by means of Attenuated Total Reflectance Fourier Transform Infrared (ATR-FTIR) spectroscopy in a ThermoScientific Nicolet iS10 apparatus with a Smart iTR-Diamond module and OMNIC software in the 4000–650 cm^{-1} range with a resolution of 4 cm^{-1}. Micro-Fourier Transform Infrared Spectroscopy (micro-FTIR) was performed in a Perkin-Elmer Spotlight 200 Spectrum Two apparatus with MCT detector operating in transmission mode. The measurement procedure required individually placing the particles on KBr discs using a zircon microneedle. The resolution and spectral range were 8 cm^{-1} and 4000-550 cm^{-1} respectively. DLS measurements were performed using a Malvern Zetasizer Nano ZS instrument using backscatter detection and Non-Negative Least Squares fitting algorithm. Total Organic Carbon (TOC) was determined as NPOC, using a Shimadzu TOC-VCSH apparatus equipped with ASI-V autosampler. Differential Scanning Calorimetry (DSC) analyses were performed using a DSC/DTA/TGA Q600 module from TA Instruments with heating rate 10 °C/min. Melting temperature, T_m, was obtained from the heating curve and crystallinity from the ratio of the melting enthalpy of the sample taken the melting enthalpy of fully crystalline PE as 290 kJ/kg. The morphology of pellets before and after treatments was studied using scanning electron microscopy on gold-sputtered specimens (SEM, Zeiss DSM-950 operating at 25 kV).

2.4. Flow cytometry measurements

In flow cytometry, the laser light scattered from particles is recorded in forward or side scattering angles and can be used to quantify objects in the 0.5-40 μm (Primpke et al., 2020). However very few studies have used this technique to quantify MPs (Kaile et al., 2020). The main reason is that deriving size information from scatter intensities is not straightforward. Mie's scattering theory allows calculating the angular distribution of scattered light by spherical particles, but several variables like laser intensity, quantum efficiency of the detector, and user-defined variables, make difficult to handle the scattering intensities obtained as output from flow cytometers (Welsh et al., 2020). Besides, the intensity of light scattering depends not only on particle size but also on their refractive index, which is an issue if the nature of particles is unknown or if they have complex structure (Agagliate et al., 2018).

Recently, a theoretical background using Mie's theory has been provided to derive the size of extracellular vesicles from the scattering intensity based on a previous calibration with beads of known size and refractive index (de Rond et al., 2018). The calculation is based on relating forward-scattered light (FSC) or side-scattered light (SSC) to the scattering cross-section of the particle, σ_s, which represents the power scattered over the amount of power per unit area of the incident light. The procedure relates scattered intensities to

particle size and refractive index and allows interconverting the intensity scattered by particles with different refractive index. A set of particles of known size and refractive index were used to calibrate the scattering intensities as read by the instrument (FSC or SSC) as follows:

1) PS latex beads of 1, 3, 4, 6, 10, 15 and 25 µm were used to derive a relationship between FSC (or SSC) and particle size (Fig. S2A, SM). For intermediate sizes, an interpolation allowed calculating the scattered intensity, I_{FSC} or I_{SSC}.
2) Mie's theory was used to derive scattering cross-sections for PS (n = 1.6113 at 488 nm) and LDPE (n = 1.5075 at 488 mn) as a function of size. Therefore, $(\sigma_s)_{PE}$ and $(\sigma_s)_{PS}$ can be computed for every particle size (Fig. S2B, SM).
3) The scaling factor that relates the measured scattering intensity to the theoretical scattering cross-section is the same for particles with different refractive index (de Rond et al., 2018). Therefore, scattering intensities are proportional to the scattering cross-section as follows:

$$\frac{(I_{FSC-SSC})_{LDPE}}{(I_{FSC-SSC})_{PS}} = \frac{(\sigma_s)_{LDPE}}{(\sigma_s)_{PS}} \quad [1]$$

$(I)_{LDPE}$ can be readily derived using Eq. 1 for any desired particle size. In other words, the scattering intensity (FSC or SSC) for LDPE can be obtained for any particle size within the calibration range. In this work we computed LDPE sizes in the 1-5 µm, and 5-25 µm ranges (as well as particles > 25 µm, which were those with scattering intensities higher than that calculated for 25 µm LDPE particles) as shown in Fig. S2C (SM). An example in given in Fig. S3 (SM) showing the tree regions indicated before. It is also apparent that a high number of particles < 1 µm existed in the sample.

The assumptions made for this calculation are that particles are spherical and homogeneous with refractive index coincident with the one reported for bulk material. For PS beads these assumptions offer no issues, but the particles produced during the photooxidative ageing of MPs are not expected to be spherical or homogeneous. In that case, the obtained diameter would be that of the equivalent sphere with the same scattering behaviour and refractive index. The water used for suspending the MP materials was also analysed as contamination control and to subtract any possible background signal as explained below (Renner et al., 2021).

2.5. Nanoplastic measurements

Dynamic Light Scattering (DLS) measurements were performed to assess the presence of submicron particles in the liquid samples taken at different times and filtered using 1 µm pore size Puradisc 25 TF filters. For it, aliquots of 50 mL were taken from the liquid at the end of the runs after removing the pellets, filtered using 1 µm pore size filters, concentrated in vacuum oven at 60 °C, dissolved in xylene, and reprecipitated to obtain particles that could be inspected using micro-FTIR technique. Besides, pellets from LDPE-1, 2 & 3 were dissolved in xylene, filtrated using 1 µm pore filters, and concentrated using the same procedure until obtaining a solid deposit suitable for micro-FTIR analysis, which served to compare micro-FTIR signals from < 1 µm filtrates with spectra representative of the bulk composition of the pellets, not only the outer layer accessible to ATR-FTIR.

3. Results and discussion

3.1. Effects on microplastic fragments

The ATR-FTIR spectra of LDPE pellets showing the typical peaks of PE spectrum are presented in Fig. S4 (SM). The main peaks corresponded to the stretching vibrations of $-CH_2$ at 2920 cm^{-1} and 2846 cm^{-1}, the bending mode of the $-CH_2$ between 1474 cm^{-1} and 1460 cm^{-1} (in the lower range for LDPE). The bending of $-CH_3$ terminal groups appeared around 1370 cm^{-1} and is visible only in LDPE (absent in HDPE). The $-CH_2$ rocking vibration in amorphous and crystalline domains, respectively was clear at 719 cm^{-1} and 729 cm^{-1} (Hamzah et al., 2018). Besides, the carbonyl stretching vibration visible in LDPE-2 & 3 at 1715-1735 cm^{-1}, reflected some degree of degradation of laboratory LDPE flasks and the pellets made from recycled LDPE.

Degradation indexes quantifying the presence of hydroxyl (HO), carbonyl (C=O), and carbon-oxygen bonds (C-O) have been calculated as the ratio of peak(s) height, expressed as absorbance, to the height of a reference peak, both from corrected baseline. The reference taken in this work was the 2920 cm^{-1} main stretching vibration of $-CH_2$, that has been shown to be relatively insensitive to polymer ageing (Brandon et al., 2016). The bands generally selected for hydroxyl, carbonyl, and carbon-oxygen bonds are 3200-3500 cm^{-1}, 1550-1810 cm^{-1} and 1000-1200 cm^{-1} respectively. The presence of carbonyl bands is particularly relevant. The photochemical degradation of PE is known to proceed through various steps, beginning by the formation of ketones followed by carboxylic acids, esters, and lactones at wavenumbers in the 1713-1780 cm^{-1} range (Gardette et al., 2013). We took for carbonyl index, the highest peak in that area. For the quantification of carbon-oxygen bonds, we used the peaks at 1160 cm^{-1} and 1230 cm^{-1} attributed to C-O-C and C-O stretching vibrations.

Table 1 shows the evolution of the three degradation indexes (OH, C=O and C-O) for pellets taken at different times and for fragments recovered in 25 µm filters at the end of the runs. All indexes, calculated as average of at least three readings on different specimens from at least two experiments, displayed a tendency to

increase with the time in contact with water and with irradiation time. The highest values corresponded to irradiated samples and, especially, to the small MP fragments detached from pellets during the runs and recovered onto 25 μm filters. The presence of oxygenated moieties was clearly observed. These findings are in agreement with the well-known fact that the degradation of PE initiated by oxygen in combination with light, heat or mechanical stress is mediated by oxygen-containing radicals (Zhu et al., 2018). The mechanism of photoinitiated degradation of PE is known to proceed when UV-light breaks bonds on the polymer backbone followed by propagation steps in which the newly formed radicals take oxygen to form peroxyl radicals. Propagation reactions take place via hydrogen transfer or after the formation of alkoxy radicals eventually leading to the generation of hydroxyl groups (Smith et al., 2018). Subsequent reactions result to chain scission or crosslinking with the production of oxygenated specific oxygen-containing functional groups like aliphatic carboxylic acids, aldehydes, and ketones (Gewert et al., 2015). This scenario is consistent with the facts that all degradation indexes increased with time and that C-O index did not reach high values for some irradiated runs. In the absence of UV radiation, heat and mechanical also lead to the formation of oxygenated moieties that also increase the rate of hydrolysis like carbonyl bonds, which are hydrolytically susceptible. Besides, the initial formation of reactive moieties may take place during processing or manipulation and is most probably the reason for the relatively high oxidation indexes observed for LDPE-3-[0].

Table 1. Hydroxyl (HO), carbonyl (C=O), and carbon-oxygen bond (C-O) indexes calculated from ATR-FTIR and micro-FTIR, melting temperature (T_m), and crystallinity (X) from DSC data. (Values are given with standard deviation; NS: Not significantly different from zero.)

	HO index	C=O index	C-O index	T_m (°C)	X(%)
Pellets (ATR-FTIR)					
LDPE-1-[0]	-	-	-	117.8 ± 0.2	44.0 ± 0.8
LDPE-1-[24]-NI	NS	NS	0.109 ± 0.018	117.1 ± 0.3	48.1 ± 0.6
LDPE-1-[48]-NI	NS	NS	0.276 ± 0.022	115.5 ± 0.2	47.9 ± 0.5
LDPE-1-[72]-NI	NS	0.016 ± 0.009	0.452 ± 0.031	110.9 ± 0.4	44.6 ± 1.2
LDPE-1-[24]-I	NS	NS	0.184 ± 0.014	116.3 ± 0.5	45.0 ± 0.9
LDPE-1-[48]-I	NS	0.017 ± 0.011	0.273 ± 0.023	116.0 ± 0.3	46.9 ± 1.4
LDPE-1-[72]-I	0.010 ± 0.008	0.023 ± 0.014	0.289 ± 0.027	114.0 ± 0.4	49.7 ± 1.6
LDPE-2-[0]	0.012 ± 0.007	NS	0.025 ± 0.016	110.9 ± 0.4	45.4 ± 0.8
LDPE-2-[24]-NI	0.009 ± 0.005	NS	0.057 ± 0.021	110.2 ± 0.3	41.0 ± 1.1
LDPE-2-[48]-NI	NS	0.017 ± 0.011	0.173 ± 0.014	109.8 ± 0.3	40.2 ± 0.9
LDPE-2-[72]-NI	NS	0.026 ± 0.015	0.290 ± 0.023	107.9 ± 0.5	40.0 ± 1.3
LDPE-2-[24]-I	0.018 ± 0.010	NS	0.146 ± 0.017	108.8 ± 0.1	39.8 ± 1.5
LDPE-2-[48]-I	0.014 ± 0.008	0.016 ± 0.009	0.255 ± 0.020	108.0 ± 0.2	40.4 ± 1.4
LDPE-2-[72]-I	0.015 ± 0.011	0.022 ± 0.012	0.289 ± 0.021	107.9 ± 0.4	40.7 ± 0.9
LDPE-3-[0]	NS	0.070 ± 0.017	0.093 ± 0.031	117.0 ± 0.2	40.1 ± 0.6
LDPE-3-[24]-NI	0.016 ± 0.012	0.075 ± 0.032	0.166 ± 0.027	115.5 ± 0.3	40.6 ± 0.8
LDPE-3-[48]-NI	0.025 ± 0.010	0.080 ± 0.012	0.411 ± 0.051	114.8 ± 0.2	39.6 ± 1.1
LDPE-3-[72]-NI	0.038 ± 0.008	0.097 ± 0.016	0.462 ± 0.034	113.3 ± 0.4	39.1 ± 2.3
LDPE-3-[24]-I	0.012 ± 0.009	0.067 ± 0.021	0.113 ± 0.022	115.5 ± 0.3	38.6 ± 1.8
LDPE-3-[48]-I	0.022 ± 0.014	0.076 ± 0.008	0.141 ± 0.008	115.5 ± 0.3	39.5 ± 1.4
LDPE-3-[72]-I	0.041 ± 0.018	0.092 ± 0.015	0.281 ± 0.016	113.3 ± 0.4	40.0 ± 1.9
Small fragments (> 25 μm, micro-FTIR)					
LDPE-1-[72]-NI	NS	0.009 ± 0.007	0.137 ± 0.029	-	-
LDPE-1-[72]-I	0.028 ± 0.008	0.031 ± 0.011	0.353 ± 0.024	-	-
LDPE-2-[72]-NI	0.039 ± 0.014	0.098 ± 0.026	0.115 ± 0.057	-	-
LDPE-2-[72]-I	0.124 ± 0.021	0.170 ± 0.032	0.308 ± 0.062	-	-
LDPE-3-[72]-NI	0.076 ± 0.024	0.118 ± 0.028	0.074 ± 0.025	-	-
LDPE-3-[72]-I	0.152 ± 0.038	0.312 ± 0.051	0.476 ± 0.054	-	-

Fig. 1 shows the micro-FTIR spectra of small MPs detached from the pellets with all bands corresponding to oxygenated moieties clearly visible. Higher degradation was observed for small fragments in comparison with pellets because small MPs are more prone to undergo hydrolytic and photooxidative reactions and because the surface of pellets exposed after the detachment of secondary fragments should be less aged. Besides, the different technique used, transmittance micro-FTIR for small fragments, and ATR-FTIR for pellets needs to be considered. The penetration depth of ATR-FTIR depends on several factors, namely wavelength, angle of incidence, and the refractive indexes of the crystal used and the sample. Overall, the sampling depth of the method is approximately in the 2-15 μm range, higher for decreasing wavenumber (Larkin, 2011). Specifically, for the equipment used in this work, with angle of incidence 42°, diamond prism (refractive index 2.4) and for LDPE (refractive index 1.5), the penetration depth is in the range 0.5 μm (4000 cm^{-1}) to 5.0 μm (400 cm^{-1}). The relative protection of the inner parts of the plastic has been described before, as a factor to take into account when using oxidation indexes to assess the weathering of plastics taken from the environment (Brandon et al., 2016). Although the comparison with other works is difficult due to the use of different reference bands and peak area instead of peak height, the results reported here are in line with those found for PE materials aged under UV- or Xe-arc light (Gulmine et al., 2003; Stark and Matuana, 2004). Fig. S5 (SM) shows images of small MPs fragments recovered on 25 μm filters from which micro-FTIR spectra were recorded.

Table 1 also shows melting temperature, T_m, and the degree of crystallinity of pellets taken at different times from DSC measurements. Melting temperature showed a slight tendency to decrease with lowest values at the end of the runs, which could be explained by the increase in crystal defects that take place during oxidative degradation upon the incorporation of oxygenated moieties, chain ends, and branching sites, all of them originating smaller and less perfect crystals (Ojeda et al., 2011). Crystallinity, however displayed little changes with a certain tendency to increase upon irradiation. It has been shown that UV irradiation generates bulkier oxygen-containing groups that increase interchain distance, therefore decreasing crystallinity. However, the structural modifications occurring during PE ageing are complex and some factors lead to a crystallinity increase and others to the opposite (Carrasco et al., 2001). The limited usefulness of crystallinity to assess PE ageing agrees with data reported elsewhere (Brandon et al., 2016). DSC plots are given in Fig. S6 (SM).

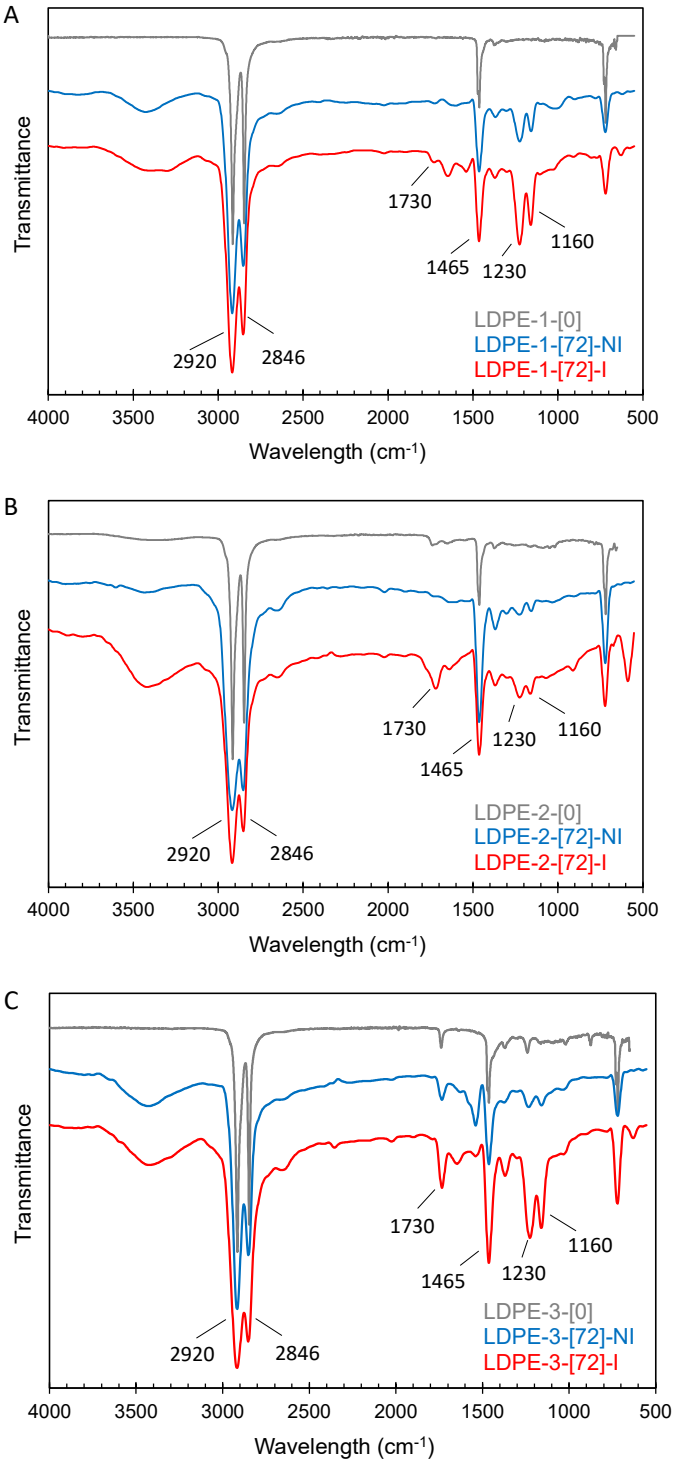

Figure 1. Micro-FTIR spectra for the fragments retained by 25 μm filters indicating the main peaks used for the calculations shown in Table 1. The spectra of the original materials LDPE-1 (A), 2 (B) & 3 (C) are also shown.

3.2. Fragmentation into smaller microplastics

In the environment, MPs undergo fragmentation processes that release smaller plastic fragments. While photodegradation has been considered the principal formation pathway for the degradation of plastics in the environment, other studies suggested that mechanical and even biological fragmentation may play a significant role. A recent evidence was provided that Antarctic krill, through their digestive system, could be

fragmentating PE microbeads into smaller fragments (Dawson et al., 2018). The combination of oxidative degradation with mechanical stress was studied for expanded polystyrene (EPS) in laboratory simulations that included the nanoplastic size fraction measured by nanoparticle tracking analysis. The study concluded that mechanical fragmentation is an important environmental process leading to the formation of secondary particles, even nanoparticles in the few hundred of nanometres range (Mattsson et al., 2021). It has also been shown that polyester synthetic fibres undergo degradation and fragmentation due to a combination of photooxidation and mechanical abrasion, possibly with degradation being UV-initiated (Sørensen et al., 2021). Overall, the fragmentation of MPs is a complex process that could be attributed to the combined action of tensile stresses and the loss of mechanical properties due to polymer hydrolysis and photodegradation (ter Halle et al., 2016). Wahl et al. demonstrated the plastic degradation including the generation of NPs can take place in soil suggesting the implication of mechanisms different from photooxidative processes (Wahl et al., 2021). Accelerated weathering experiments combining UV exposure with mechanical abrasion showed that polyolefins were fragmented mainly due to UV irradiation, which resulted in thousands of particles per pellet after prolonged exposure, while EPS was more affected by mechanical fragmentation (Song et al., 2017).

The ageing of polymers most probably begins by an alteration of the outer surface that leads to crack formation and propagation (Zhang et al., 2021). The SEM images of LDPE-1, 2 & 3 pellets in irradiated and non-irradiated runs showed the appearance of surface cracks and irregularities that most probably resulted in the detaching of fragments from the outer surface (Fig. S7, SM). Fig. 2 presents the number of particles in the 1-5 μm, 5-25 μm and > 25 μm ranges obtained from flow cytometry measurements as explained before and expressed per unit mass of exposed LDPE. In all cases, the background from ultrapure water was subtracted to account for possible particles driven by the MilliQ water, which represented in all cases a very minor number of particles. The results showed a high number of particles in the lower size range, with values in the tens of secondary MPs per mg of PE. It is interesting to point out that this size range, as low as 1 μm, is lower than that reported in most studies. The limit for FTIR imaging, even improved by the focal plane array (FPA)-based technology is still in the 10 μm range, and the accuracy considerably decreases for particles < 50 μm (Simon et al., 2018; Yang et al., 2021). Raman microscopy allows approaching the lower limit of MPs, in the few microns range, but the technique has important drawbacks like long measurement time and difficulty to process samples with fluorescence, which appears in most polymers (Araujo et al., 2018). As a consequence, there are very limited evidence on the occurrence of small MPs in the environment, although different studies demonstrated that small MPs are much more abundant than larger fragments (Eo et al., 2018; Missawi et al., 2020).

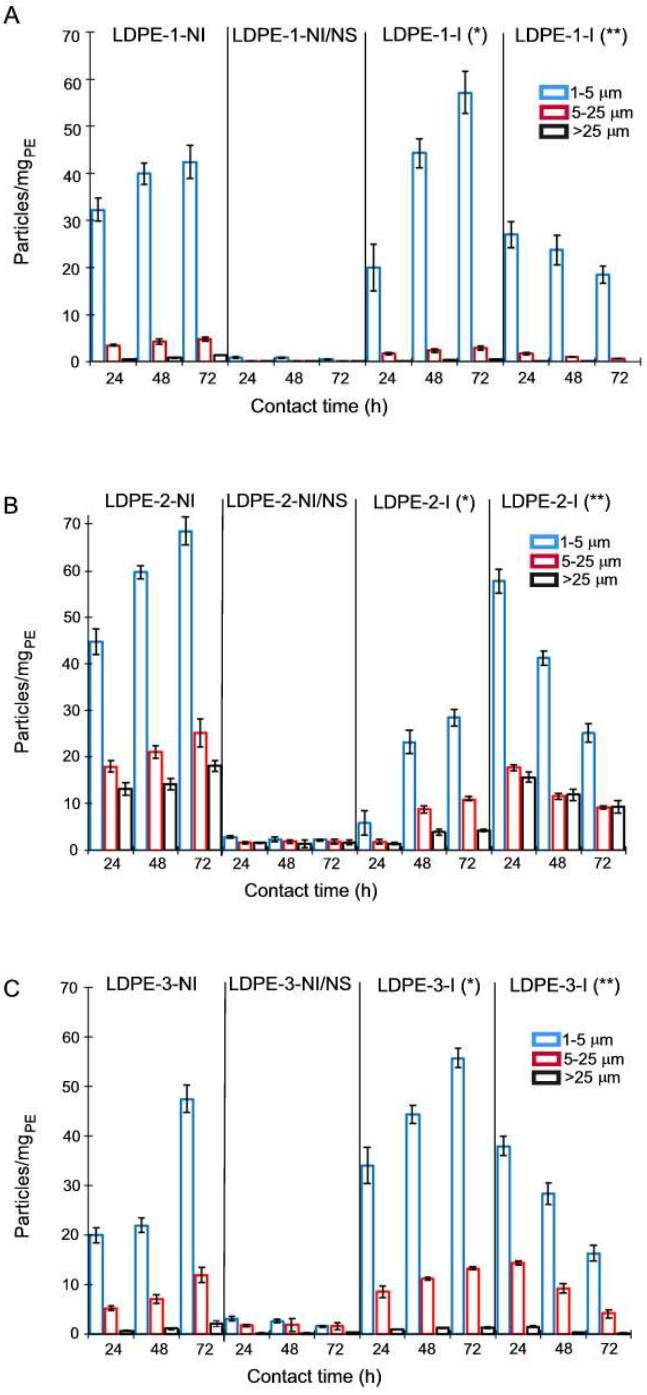

Figure 2. Particle size distribution obtained from flow cytometry experiments with LDPE-1 (A), LDPE-2 (B) and LDPE-3 (C). One asterisk (*) means Procedure I: samples irradiated and stirred for 72 h in the presence of pellets; two asterisks (**) mean Procedure II: samples irradiated and stirred for 72 h without pellets after 72 h in water in darkness with pellets. NI/NS refers to non-irradiated/non-stirred samples.

The results showed that mechanical stress played an important role in the detachment of secondary MP particles. The number of MPs produced in the absence of agitation (NI/NS runs) was very low, in the order of

units of MP/mg PE, that appeared at the beginning of the experiments and remained with little changes during the 72 h runs. These were most probably particles coming from an already altered surface that detached form larger pellets and fragments upon swelling after water immersion. The results also showed that the number of small MPs particles formed during the weathering of plastic pellets, decreased when exposed to UV light in the absence of the parent LDPE particles. This finding is clear observing the results from Procedure II, which is a continuation of non-irradiated runs for additional three-day periods after removing the pellets (Figure 2, experiments marked as Procedure II). This phenomenon affected all particle sizes and suggested that particles < 1 μm were produced during the irradiation of the MPs released during the previous 72 h stirred in darkness (as suggested by flow cytometry plots like the one showed in Fig. S3, SM). Besides, in irradiated runs with pellets, the number of fragments in the 5-25 μm range and > 25 μm tended to increase with time. However, in runs for which pellets were removed before irradiation all size ranges decreased, suggesting that UV irradiation is key for the ripping of MP into smaller particles and NPs. It was also noticeable that many small MPs appeared during the first 24 h, showing that the onset of fragmentation is rapid and does not require extensive photooxidation of the polymer surface. This phenomenon is probably due to the plasticizer effect of water (Julienne et al., 2019). The higher number of small MPs produced from LDPE-2 might be due to their higher external surface, 2210 mm^2/g, 15-20 % higher that LDPE-1/3 pellets. The higher generation of small MPs in the case of LDPE-2 was in line with the reduction in the concentration of 1-5 μm fragments when removing the pellets from the reactor. The reason is probably the ongoing degradation of larger particles, including those > 25 μm like those shown in Fig. S5. Overall, and considering all LDPE materials, the small MPs in the 1-25 μm range, quantified by flow cytometry were in the 10^6-10^7 MPs/L range, or, expressed per unit mass of polymer, 10^4-10^5 MPs/g_{PE}, which represented in all cases < 0.01 % of the exposed polymer.

3.3. Generation of nanoplastics

The fragmentation of plastic particles does not limit to micron size particles. Little is known about the lower sizes, because of the lack of established analytical methods able to detect them in the environment (Koelmans et al., 2015). In the absence of field data, laboratory studies showed that environmental factors

Table 2. TOC of samples filtered through 1 μm pore size filters and non-filtered (the numbers in brackets represents the concentration of LDPE with the same carbon content); DLS particles size from samples filtered through 1 μm filters.

		TOC (mg/L) non-filtered	TOC < 1 μm (mg/L)	DLS particle size, filtered < 1 μm (nm)
Non-irradiated (darkness)	LDPE-1-[24]-NI	1.9 (2.2) ± 0.2	-	258 ± 11
	LDPE-1-[48]-NI	2.1 (2.5) ± 0.3	-	231 ± 14
	LDPE-1-[72]-NI	2.3 (2.7) ± 0.2	1.7 (2.0) ± 0.2	220 ± 12
	LDPE-2-[24]-NI	5.5 (6.4) ± 2.1	-	244 ± 22
	LDPE-2-[48]-NI	7.4 (8.6) ± 2.2	-	242 ± 13
	LDPE-2-[72]-NI	9.2 (10.7) ± 2.4	5.0 (5.8) ± 2.2	142 ± 15
	LDPE-3-[24]-NI	2.4 (2.8) ± 0.5	-	200 ± 24
	LDPE-3-[48]-NI	3.2 (3.7) ± 0.7	-	165 ± 12
	LDPE-3-[72]-NI	3.6 (4.2) ± 0.5	2.7 (3.2) ± 0.7	158 ± 17
Irradiated	LDPE-1-[24]-I	16.2 (18.9) ± 2.1	-	416 ± 20
	LDPE-1-[48]-I	18.2 (21.2) ± 3.2	-	371 ± 16
	LDPE-1-[72]-I	20.5 (23.9) ± 2.2	18.9 (22.1) ± 2.5	328 ± 19
	LDPE-2-[24]-I	24.3 (28.4) ± 5.2	-	636 ± 92 104 ± 17
	LDPE-2-[48]-I	34.6 (40.4) ± 6.1	-	307 ± 17
	LDPE-2-[72]-I	39.6 (46.2) ± 4.2	38.5 (44.9) ± 7.8	279 ± 14
	LDPE-3-[24]-I	6.2 (7.2) ± 1.3	-	192 ± 42
	LDPE-3-[48]-I	7.7 (9.0) ± 1.5	-	167 ± 23
	LDPE-3-[72]-I	8.8 (10.3) ± 1.8	5.0 (5.8) ± 1.5	160 ± 18

led to the production of nanosized plastic particles (Rios Mendoza et al., 2018; Song et al., 2020). Gigault et al. used a photoreactor emitting UVA + UVB with irradiance 1000 W m^{-2}, essentially the same used in this work, to demonstrate de the formation of NPs from the degradation of marine microplastics. The results, obtained using DLS and TEM for particle characterization, suggested that the smaller NP particles were produced after the initial formation of larger plastic particles (Gigault et al., 2016). In our runs, DLS measurements in the liquid samples taken at different times showed the presence of colloidal submicron particles as indicated in Table 2. DLS plots for samples irradiated for 72 h are shown in Fig. S8 (SM). Clear peaks in the few hundreds of nm appeared in all DLS plots with a slight tendency to size decrease with time and larger nanoparticles in irradiated samples. This was probably due to the higher input of newly formed nanoparticles, but this assumption has to be handled with care because of the limited sensitivity of DLS in the case of polydisperse colloids. As in the case of larger secondary MPs, no aggregation pattern was observed, with stable DLS particle size even when repeating the measurement days after the run. Table 2 also shows the TOC of samples, filtered through 1 µm filters, and without filtration. In all cases, the organic carbon content was higher in irradiated samples and increased with time as expected from the role of UV irradiation in the photodegradation of polymers. As for the generation of secondary MPs, the release of organic matter was not linear with time, reflecting an early generation of NPs, which is probably related to the presence of surface defects or reactive moieties originated during the processing of storage of pellets.

The liquid concentrated form filtered aliquots taken at the end of runs was examined to assess the presence of LDPE. The extraction process described in the experimental section yielded small aggregates that could be inspected using micro-FTIR. The results are shown in Fig. 2 together with those of pellets dissolved and precipitated using the same procedure. In all cases the characteristics features of PE spectra were clearly observed, namely the peaks at 2920, 2846, 1465 and 719 cm^{-1} as indicated before. Besides, the spectra from LDPE-1, 2 & 3 displayed additional bands most probably due to additives, which appeared magnified in < 1 µm filtrates in irradiated and, to a lesser extent, in non-irradiated runs. Noteworthy, the N-H tensile absorption usually observed as two broad peaks in the 3300-3500 cm^{-1}, the two peaks of C-N stretching at about 1250-1020 cm^{-1}, and the N-H out of plane bending at 793 cm^{-1}, are visible in most spectra, probably indicating the presence of light stabilizers, which are usually based on secondary and tertiary hindered amines and that protect polymers against degradation by acting as free radical scavengers and peroxide decomposers (Beißmann et al., 2014). The presence of additives could be one of the factors explaining the differences among the three LDPE materials observed in this work. Table S1 (SM) shows the TOC for NI/NS runs, which was very low compared to the values for stirred runs listed in Table 2, indicating that mechanical agitation is needed to release most of the carbon containing substances released by the MPs. The presence of plastic fragments < 1 µm could not be assessed by DLS or spectroscopic analyses in NI/NS samples, indicating that, if produced, they were in very low concentration.

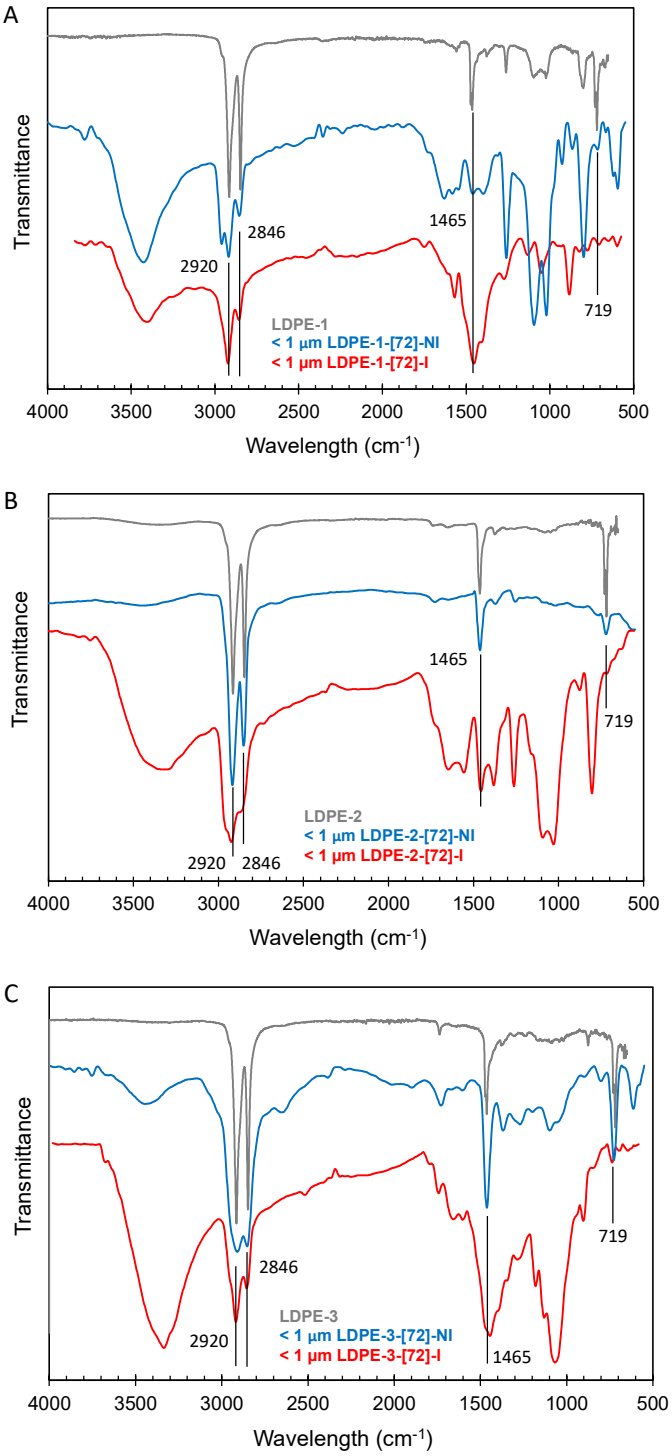

Figure 3. Micro-FTIR spectra for the fragments < 1 µm filters indicating the characteristic peaks of LDPE. The spectra of the original materials LDPE-1 (A), 2 (B) and 3 (C) are also shown.

If all organic matter consisted only of LDPE, considering the particle size given in Table 2 and using the density of PE, the concentration of NP particles would represent about 10^{10} NPs/g_{PE} (~0.10 % of the original mass of the pellet; this calculation assumes spherical particles with the average density of LDPE). The presence of oxidized groups in LDPE-derived NPs was clear from the peaks of carbonyl stretching vibration and other peaks attributed to carbon-oxygen bonds as explained before. This is the first evidence of the formation of NPs from PE under photooxidative conditions. Our results suggest that PE debris are disseminating huge amounts of NPs which are still very difficult or impossible to assess in real environmental matrixes.

4. Conclusions

In this work, we studied the hydrolytic, mechanical, and photochemical degradation of three LDPE materials exposed to the UV radiation equivalent to one year of solar UVB + UVA irradiance (280-400 nm). Flow cytometry was used for the first time to quantify the small MPs (1-25 μm) produced during the degradation of LDPE. The results showed the generation of a high number of small MPs with values reaching 10^4-10^5 MPs per gram of PE pellets in the 1-25 μm range. Mechanical degradation led to a rapid production of secondary MPs, while photochemical ageing increased the concentration of NPs (< 1 μm). FTIR studies showed clear signs of oxygenated moieties, particularly in irradiated runs, which increased with exposure time. The presence of NPs was assessed using micro-FTIR after precipitating the colloidal fraction < 1 μm into larger particles. The size of NPs, measured by DLS, was in the hundreds of nm range, and their number could represent up to 10^{10} NPs per gram of LDPE.

Acknowledgements

The authors acknowledge the financial support provided by the Spanish Government: CTM2016-74927-C2-1/2-R, and the Thematic Network of Micro- and Nanoplastics in the Environment (RED2018-102345-T, EnviroPlaNet Network).

References

Agagliate, J., Röttgers, R., Twardowski, M.S., McKee, D., 2018. Evaluation of a flow cytometry method to determine size and real refractive index distributions in natural marine particle populations. Appl. Opt. 57, 1705-1716. https://doi.org/10.1364/ao.57.001705.

Araujo, C.F., Nolasco, M.M., Ribeiro, A.M.P., Ribeiro-Claro, P.J.A., 2018. Identification of microplastics using Raman spectroscopy: Latest developments and future prospects. Water Res. 142, 426-440. https://doi.org/https://doi.org/10.1016/j.watres.2018.05.060.

Barrowclough, D., Birkbeck, C.D., Christen, J., 2020. Global trade in plastics: insights from the first life-cycle trade database, in: UNCTAD Research Paper No. 53, U.S.R. (Ed.). United Nations Conference on Trade and Development.

Beißmann, S., Reisinger, M., Grabmayer, K., Wallner, G., Nitsche, D., Buchberger, W., 2014. Analytical evaluation of the performance of stabilization systems for polyolefinic materials. Part I: Interactions between hindered amine light stabilizers and phenolic antioxidants. Polym. Degrad. Stab. 110, 498-508. https://doi.org/https://doi.org/10.1016/j.polymdegradstab.2014.09.020.

Bhagat, J., Nishimura, N., Shimada, Y., 2021. Toxicological interactions of microplastics/nanoplastics and environmental contaminants: Current knowledge and future perspectives. J. Hazard. Mater. 405, 123913. https://doi.org/https://doi.org/10.1016/j.jhazmat.2020.123913.

Brandon, J., Goldstein, M., Ohman, M.D., 2016. Long-term aging and degradation of microplastic particles: Comparing in situ oceanic and experimental weathering patterns. Mar. Pollut. Bull. 110, 299-308. https://doi.org/https://doi.org/10.1016/j.marpolbul.2016.06.048.

Carrasco, F., Pagès, P., Pascual, S., Colom, X., 2001. Artificial aging of high-density polyethylene by ultraviolet irradiation. Eur. Polym. J. 37, 1457-1464. https://doi.org/https://doi.org/10.1016/S0014-3057(00)00251-2.

Chamas, A., Moon, H., Zheng, J., Qiu, Y., Tabassum, T., Jang, J.H., Abu-Omar, M., Scott, S.L., Suh, S., 2020. Degradation rates of plastics in the environment. ACS Sustainable Chem. Eng. 8, 3494-3511. https://doi.org/10.1021/acssuschemeng.9b06635.

Dawson, A.L., Kawaguchi, S., King, C.K., Townsend, K.A., King, R., Huston, W.M., Bengtson Nash, S.M., 2018. Turning microplastics into nanoplastics through digestive fragmentation by Antarctic krill. Nat. Commun. 9, 1001. https://doi.org/10.1038/s41467-018-03465-9.

de Rond, L., Coumans, F.A.W., Nieuwland, R., van Leeuwen, T.G., van der Pol, E., 2018. Deriving extracellular vesicle size from scatter intensities measured by flow cytometry. Current Protocols in Cytometry 86, e43. https://doi.org/https://doi.org/10.1002/cpcy.43.

Eo, S., Hong, S.H., Song, Y.K., Lee, J., Lee, J., Shim, W.J., 2018. Abundance, composition, and distribution of microplastics larger than 20 μm in sand beaches of South Korea. Environ. Pollut. 238, 894-902.

https://doi.org/https://doi.org/10.1016/j.envpol.2018.03.096.
Gardette, M., Perthue, A., Gardette, J.-L., Janecska, T., Földes, E., Pukánszky, B., Therias, S., 2013. Photo- and thermal-oxidation of polyethylene: Comparison of mechanisms and influence of unsaturation content. Polym. Degrad. Stab. 98, 2383-2390. https://doi.org/https://doi.org/10.1016/j.polymdegradstab.2013.07.017.
GESAMP, 2015. Sources, fate and effects of microplastic in the marine environment: A global assessment (Part 1), in: Kershaw, P.J. (Ed.). IMO/FAO/UNESCO-IOC/UNIDO/WMO/IAEA/UN/UNEP/UNDP/ISA Joint Group of Experts on the Scientific Aspects of Marine Environmental Protection, p. 220.
GESAMP, 2016. Sources, fate and effects of microplastic in the marine environment: A global assessment (Part 2), in: Kershaw, P.J., Rochman, C.M. (Eds.). (IMO/FAO/UNESCO-IOC/UNIDO/WMO/IAEA/UN/UNEP/UNDP Joint Group of Experts on the Scientific Aspects of Marine Environmental Protection, p. 220.
GESAMP, 2019. Guidelines for the monitoring and assessment of plastic litter in the ocean, in: Kershaw, P.J., Turra, A., Galgani, F. (Eds.). IMO/FAO/UNESCO-IOC/UNIDO/WMO/IAEA/UN/UNEP/UNDP/ISA Joint Group of Experts on the Scientific Aspects of Marine Environmental Protection, p. 130.
Gewert, B., Plassmann, M.M., MacLeod, M., 2015. Pathways for degradation of plastic polymers floating in the marine environment. Environ. Sci. Processes Impacts 17, 1513-1521. https://doi.org/10.1039/C5EM00207A.
Gigault, J., Halle, A.t., Baudrimont, M., Pascal, P.-Y., Gauffre, F., Phi, T.-L., El Hadri, H., Grassl, B., Reynaud, S., 2018. Current opinion: What is a nanoplastic? Environ. Pollut. 235, 1030-1034. https://doi.org/https://doi.org/10.1016/j.envpol.2018.01.024.
Gigault, J., Pedrono, B., Maxit, B., Ter Halle, A., 2016. Marine plastic litter: the unanalyzed nano-fraction. Environ. Sci. Nano 3, 346-350. https://doi.org/10.1039/C6EN00008H.
Gonçalves, J.M., Bebianno, M.J., 2021. Nanoplastics impact on marine biota: A review. Environ. Pollut. 273, 116426. https://doi.org/https://doi.org/10.1016/j.envpol.2021.116426.
González-Pleiter, M., Tamayo-Belda, M., Pulido-Reyes, G., Amariei, G., Leganés, F., Rosal, R., Fernández-Piñas, F., 2019. Secondary nanoplastics released from a biodegradable microplastic severely impact freshwater environments. Environ. Sci. Nano 6, 1382-1392. https://doi.org/10.1039/C8EN01427B.
Gulmine, J.V., Janissek, P.R., Heise, H.M., Akcelrud, L., 2003. Degradation profile of polyethylene after artificial accelerated weathering. Polym. Degrad. Stab. 79, 385-397. https://doi.org/https://doi.org/10.1016/S0141-3910(02)00338-5.
Hamzah, M., Khenfouch, M., Rjeb, A., Sayouri, S., Houssaini, D., Darhouri, M., Srinivasu, V., 2018. Surface chemistry changes and microstructure evaluation of low density nanocluster polyethylene under natural weathering: a spectroscopic investigation. J. Phys. Conf. Ser. 984, 012010.
Hernandez, L.M., Yousefi, N., Tufenkji, N., 2017. Are there nanoplastics in your personal care products? Environ. Sci. Technol. Letters 4, 280-285. https://doi.org/10.1021/acs.estlett.7b00187.
Hiejima, Y., Kida, T., Takeda, K., Igarashi, T., Nitta, K.-h., 2018. Microscopic structural changes during photodegradation of low-density polyethylene detected by Raman spectroscopy. Polym. Degrad. Stab. 150, 67-72. https://doi.org/https://doi.org/10.1016/j.polymdegradstab.2018.02.010.
Julienne, F., Delorme, N., Lagarde, F., 2019. From macroplastics to microplastics: Role of water in the fragmentation of polyethylene. Chemosphere 236, 124409. https://doi.org/https://doi.org/10.1016/j.chemosphere.2019.124409.
Kaile, N., Lindivat, M., Elio, J., Thuestad, G., Crowley, Q.G., Hoell, I.A., 2020. Preliminary results from detection of microplastics in liquid samples using flow cytometry. Front. Mar. Sci. 7. https://doi.org/10.3389/fmars.2020.552688.
Kalogerakis, N., Karkanorachaki, K., Kalogerakis, G.C., Triantafyllidi, E.I., Gotsis, A.D., Partsinevelos, P., Fava, F., 2017. Microplastics generation: onset of fragmentation of polyethylene films in marine environment mesocosms. Front. Mar. Sci. 4. https://doi.org/10.3389/fmars.2017.00084.
Koelmans, A.A., Besseling, E., Shim, W., 2015. Nanoplastics in the aquatic environment. Critical review, in: Bergmann, M., Gutow, L., Klages, M. (Eds.), Marine Anthropogenic Litter, pp. 325-340.
Koelmans, A.A., Kooi, M., Law, K.L., van Sebille, E., 2017. All is not lost: deriving a top-down mass budget of plastic at sea. Environ. Res. Lett. 12, 114028. https://doi.org/10.1088/1748-9326/aa9500.
Larkin, P. Instrumentation and Sampling Methods, in: P. Larkin (Ed.) Infrared and Raman Spectroscopy, Elsevier, Oxford, 2011, pp. 27-54.
Larue, C., Sarret, G., Castillo-Michel, H., Pradas del Real, A.E., 2021. A critical review on the impacts of nanoplastics and microplastics on aquatic and terrestrial photosynthetic organisms. Small 17, 2005834.

https://doi.org/https://doi.org/10.1002/smll.202005834.
Mattsson, K., Björkroth, F., Karlsson, T., Hassellöv, M., 2021. Nanofragmentation of expanded polystyrene under simulated environmental weathering (thermooxidative degradation and hydrodynamic turbulence). Front. Mar. Sci. 7. https://doi.org/10.3389/fmars.2020.578178.
Missawi, O., Bousserrhine, N., Belbekhouche, S., Zitouni, N., Alphonse, V., Boughattas, I., Banni, M., 2020. Abundance and distribution of small microplastics (≤ 3 μm) in sediments and seaworms from the Southern Mediterranean coasts and characterisation of their potential harmful effects. Environ. Pollut. 263, 114634. https://doi.org/https://doi.org/10.1016/j.envpol.2020.114634.
Ojeda, T., Freitas, A., Birck, K., Dalmolin, E., Jacques, R., Bento, F., Camargo, F., 2011. Degradability of linear polyolefins under natural weathering. Polym. Degrad. Stab. 96, 703-707. https://doi.org/https://doi.org/10.1016/j.polymdegradstab.2010.12.004.
PlasticsEurope, 2020. Plastics – the Facts 2019: An analysis of European plastics production, demand and waste data. PlasticsEurope: Association of Plastics Manufacturers, Brussels.
Primpke, S., Christiansen, S.H., Cowger, W., De Frond, H., Deshpande, A., Fischer, M., Holland, E.B., Meyns, M., O'Donnell, B.A., Ossmann, B.E., 2020. Critical assessment of analytical methods for the harmonized and cost-efficient analysis of microplastics. Appl. Spectrosc. 74, 1012-1047.
Renner, K.O., Foster, H.A., Routledge, E.J., Scrimshaw, M.D., 2021. A comparison of different approaches for characterizing microplastics in selected personal care products. Environ. Toxicol. Chem. n/a. https://doi.org/https://doi.org/10.1002/etc.5057.
Rios Mendoza, L.M., Karapanagioti, H., Álvarez, N.R., 2018. Micro(nanoplastics) in the marine environment: Current knowledge and gaps. Curr. Opin. Environ. Sci. Health 1, 47-51. https://doi.org/https://doi.org/10.1016/j.coesh.2017.11.004.
Ru, J., Huo, Y., Yang, Y., 2020. Microbial degradation and valorization of plastic wastes. Front. Microbiol. 11. https://doi.org/10.3389/fmicb.2020.00442.
Simon, M., van Alst, N., Vollertsen, J., 2018. Quantification of microplastic mass and removal rates at wastewater treatment plants applying Focal Plane Array (FPA)-based Fourier Transform Infrared (FT-IR) imaging. Water Res. 142, 1-9. https://doi.org/10.1016/j.watres.2018.05.019.
Smith, L.M., Aitken, H.M., Coote, M.L., 2018. The fate of the peroxyl radical in autoxidation: how does polymer degradation really occur? Acc. Chem. Res. 51, 2006-2013. https://doi.org/10.1021/acs.accounts.8b00250.
Song, Y.K., Hong, S.H., Eo, S., Han, G.M., Shim, W.J., 2020. Rapid production of micro- and nanoplastics by fragmentation of expanded polystyrene exposed to sunlight. Environ. Sci. Technol. 54, 11191-11200. https://doi.org/10.1021/acs.est.0c02288.
Song, Y.K., Hong, S.H., Jang, M., Han, G.M., Jung, S.W., Shim, W.J., 2017. Combined effects of UV exposure duration and mechanical abrasion on microplastic fragmentation by polymer type. Environ. Sci. Technol. 51, 4368-4376. https://doi.org/10.1021/acs.est.6b06155.
Sørensen, L., Groven, A.S., Hovsbakken, I.A., Del Puerto, O., Krause, D.F., Sarno, A., Booth, A.M., 2021. UV degradation of natural and synthetic microfibers causes fragmentation and release of polymer degradation products and chemical additives. Sci. Total Environ. 755, 143170. https://doi.org/https://doi.org/10.1016/j.scitotenv.2020.143170.
Stark, N.M., Matuana, L.M., 2004. Surface chemistry changes of weathered HDPE/wood-flour composites studied by XPS and FTIR spectroscopy. Polym. Degrad. Stab. 86, 1-9. https://doi.org/https://doi.org/10.1016/j.polymdegradstab.2003.11.002.
ter Halle, A., Ladirat, L., Gendre, X., Goudouneche, D., Pusineri, C., Routaboul, C., Tenailleau, C., Duployer, B., Perez, E., 2016. Understanding the fragmentation pattern of marine plastic debris. Environ. Sci. Technol. 50, 5668-5675. https://doi.org/10.1021/acs.est.6b00594.
Thompson, R.C., Moore, C.J., vom Saal, F.S., Swan, S.H., 2009. Plastics, the environment and human health: current consensus and future trends. Philos. Trans. R. Soc. London, Ser. B 364, 2153-2166. https://doi.org/10.1098/rstb.2009.0053.
Wahl, A., Le Juge, C., Davranche, M., El Hadri, H., Grassl, B., Reynaud, S., Gigault, J., 2021. Nanoplastic occurrence in a soil amended with plastic debris. Chemosphere 262, 127784. https://doi.org/https://doi.org/10.1016/j.chemosphere.2020.127784.
WEF, 2016. The new plastics economy: Rethinking the future of plastics, in: Neufeld, L., Stassen, F., Sheppard, R., Gilman, T. (Eds.), World Economic Forum. World Economic Forum, Geneve, Switzerland.
Welsh, J.A., Horak, P., Wilkinson, J.S., Ford, V.J., Jones, J.C., Smith, D., Holloway, J.A., Englyst, N.A., 2020. FCMPASS Software Aids Extracellular Vesicle Light Scatter Standardization. Cytometry Part A 97, 569-581. https://doi.org/https://doi.org/10.1002/cyto.a.23782.
Yang, L., Zhang, Y., Kang, S., Wang, Z., Wu, C., 2021. Microplastics in freshwater sediment: A review on methods, occurrence, and sources. Sci. Total

Environ. 754, 141948. https://doi.org/https://doi.org/10.1016/j.scitotenv.2020.141948.
Zhang, K., Hamidian, A.H., Tubić, A., Zhang, Y., Fang, J.K.H., Wu, C., Lam, P.K.S., 2021. Understanding plastic degradation and microplastic formation in the environment: A review. Environ. Pollut. 274, 116554. https://doi.org/https://doi.org/10.1016/j.envpol.2021.116554.
Zhu, W., Zhang, G., Liu, B., Chung, T.C.M., 2018. Polyethylene containing antioxidant moieties exhibiting high thermal-oxidative stability for high temperature applications. Polymer 146, 101-108. https://doi.org/https://doi.org/10.1016/j.polymer.2018.05.019.

Supplementary Material

Generation of nanoplastics during the photoageing of low-density polyethylene

Carmen Sorasan[1], Carlos Edo[1], Miguel González-Pleiter[2], Francisca Fernández-Piñas[2], Francisco Leganés[2], Antonio Rodríguez[1], Roberto Rosal[1,*]

1 Department of Analytical Chemistry, Physical Chemistry and Chemical Engineering, University of Alcalá, Alcalá de Henares, E-28871 Madrid, Spain

2 Department of Biology, Faculty of Sciences, Universidad Autónoma de Madrid, Cantoblanco, E-28049 Madrid, Spain

* Corresponding author: roberto.rosal@uah.es

Contents:

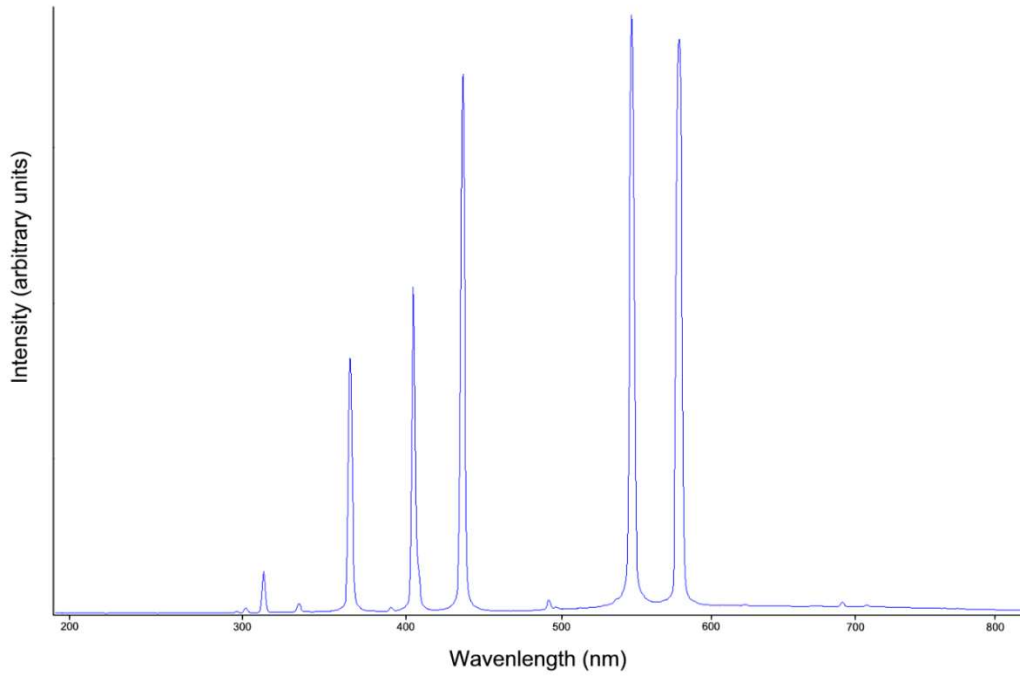

Figure S1. Emission spectrum of the Hg medium pressure lamp used in this study.

A

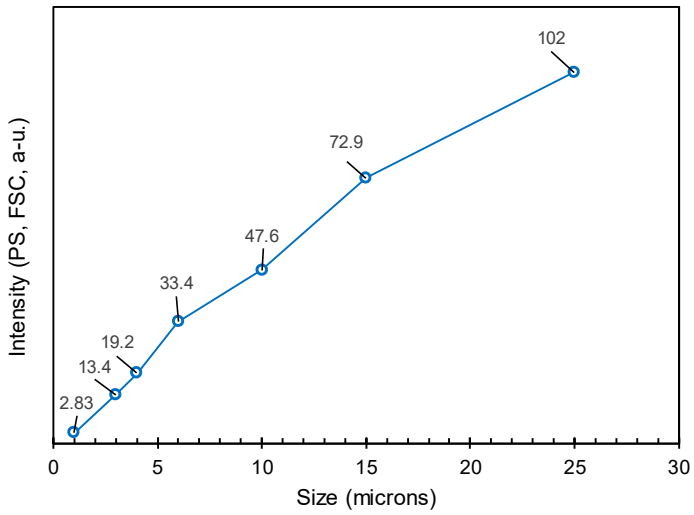

B

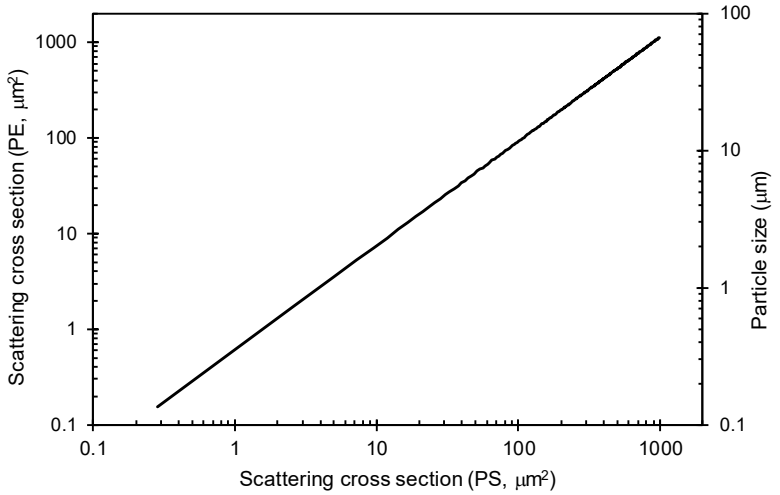

C

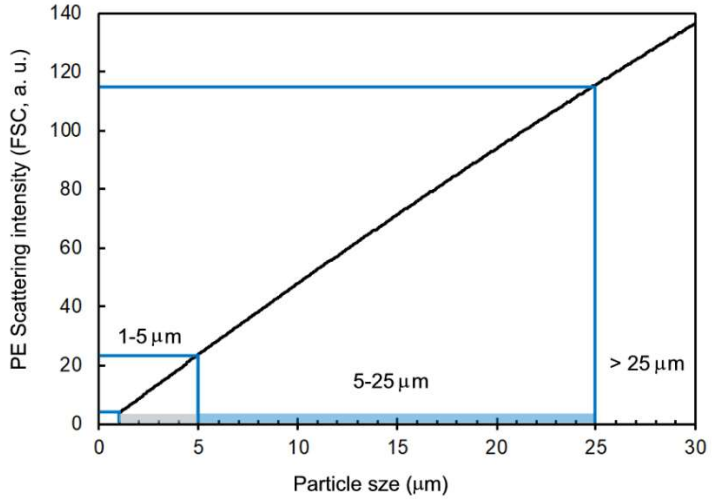

Figure S2. Intensity (FSC)-size plot for the 1, 3, 4, 6, 10, 15 and 25 μm latex beads used for calibration (A); scattering cross-sections of LDPE and PS particles as a function of size according

to Mie's theory (B); scattering intensities (FSC) calculated for LDPE and ranges of sizes studied in this work (C).

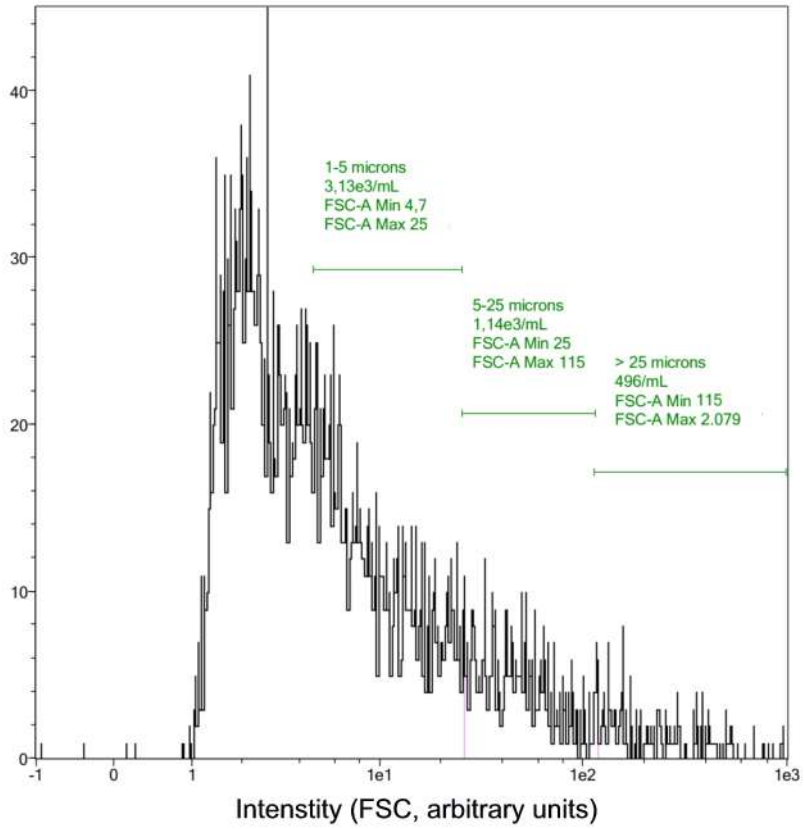

Figure S3. Example of the application of the 1-5-25 μm boundaries to the plot of LDPE-2-[72]-I taken as example.

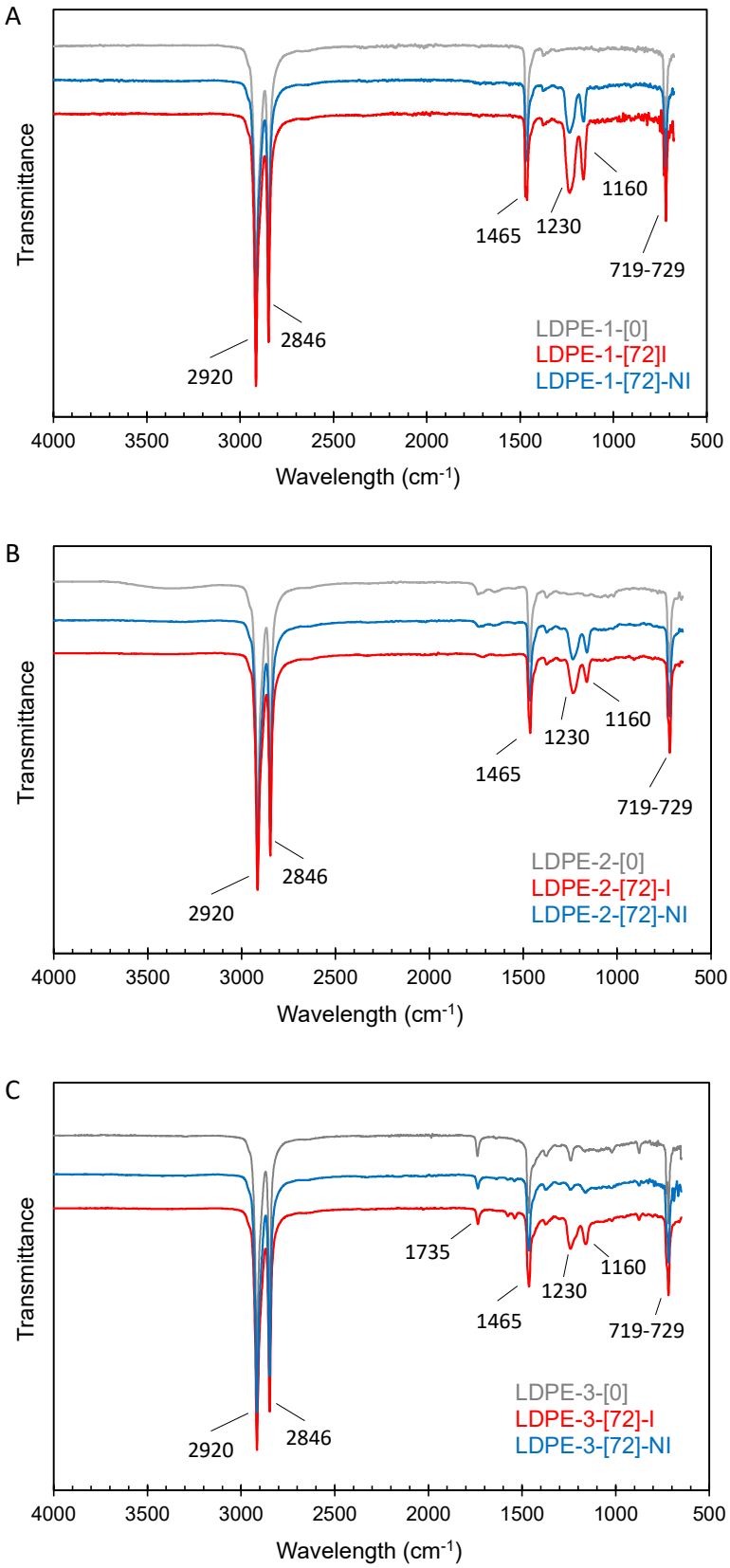

Figure S4. ATR-FTIR spectra for the pellets recovered after 72 h from irradiated and non-irradiated experiments: LDPE-1 (A), LDPE-2 (B) and LDPE-3 (C).

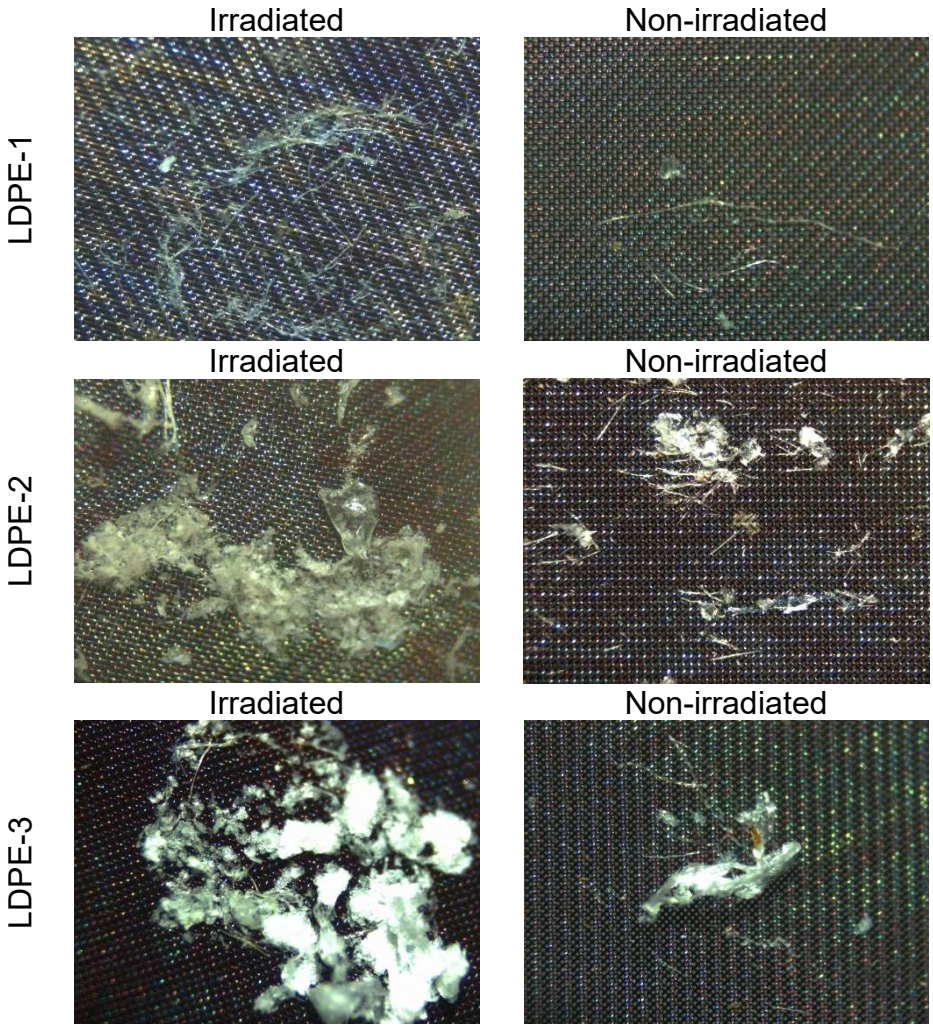

Figure S5. Images of MPs fragments recovered on 25 μm stainless steel filters for samples taken after 72 h in irradiated and non-irradiated runs (LDPE-1/2/3-[72]-I/NI).

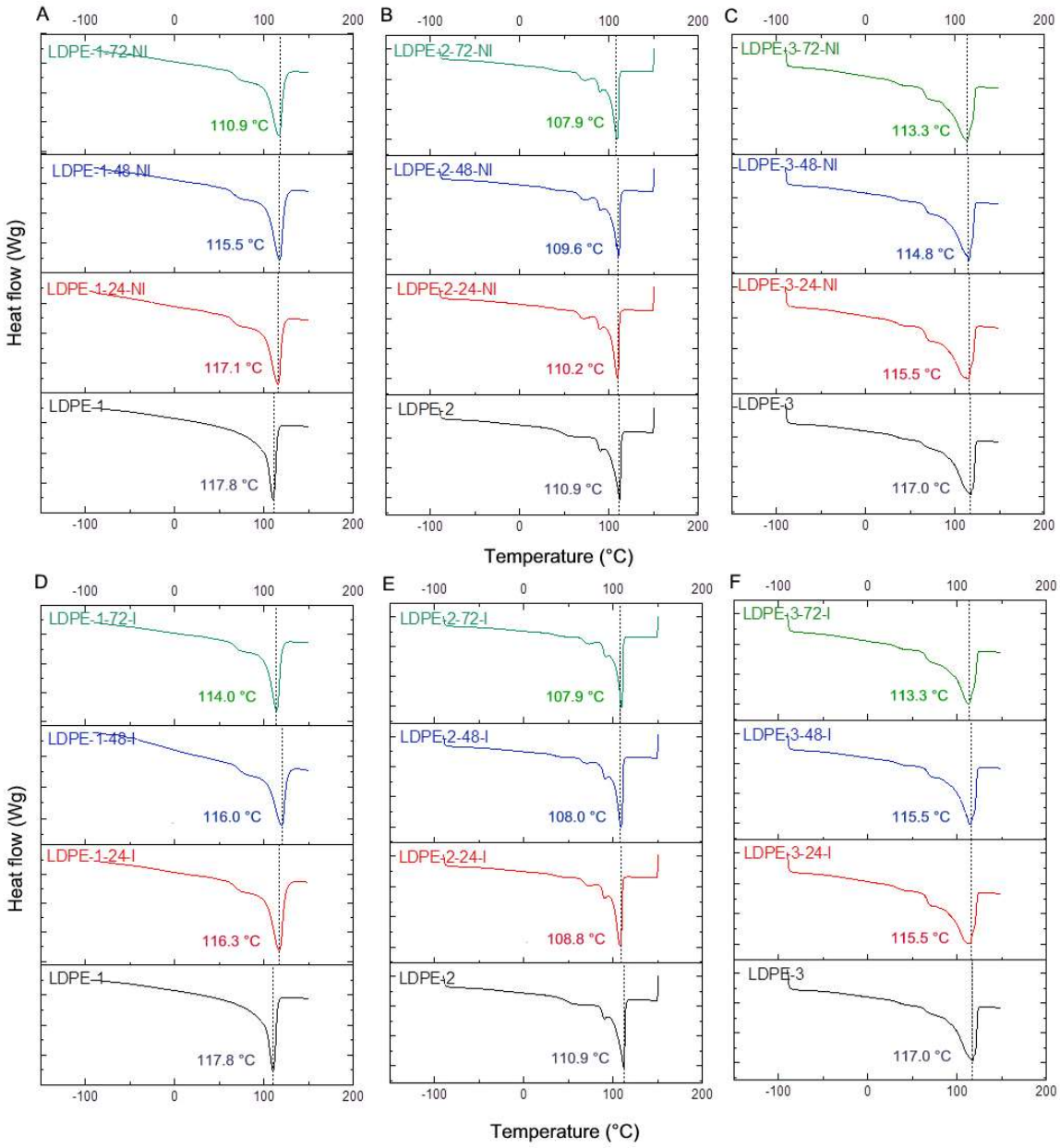

Figure S6. DSC plots of LDPE specimens recovered during the runs.

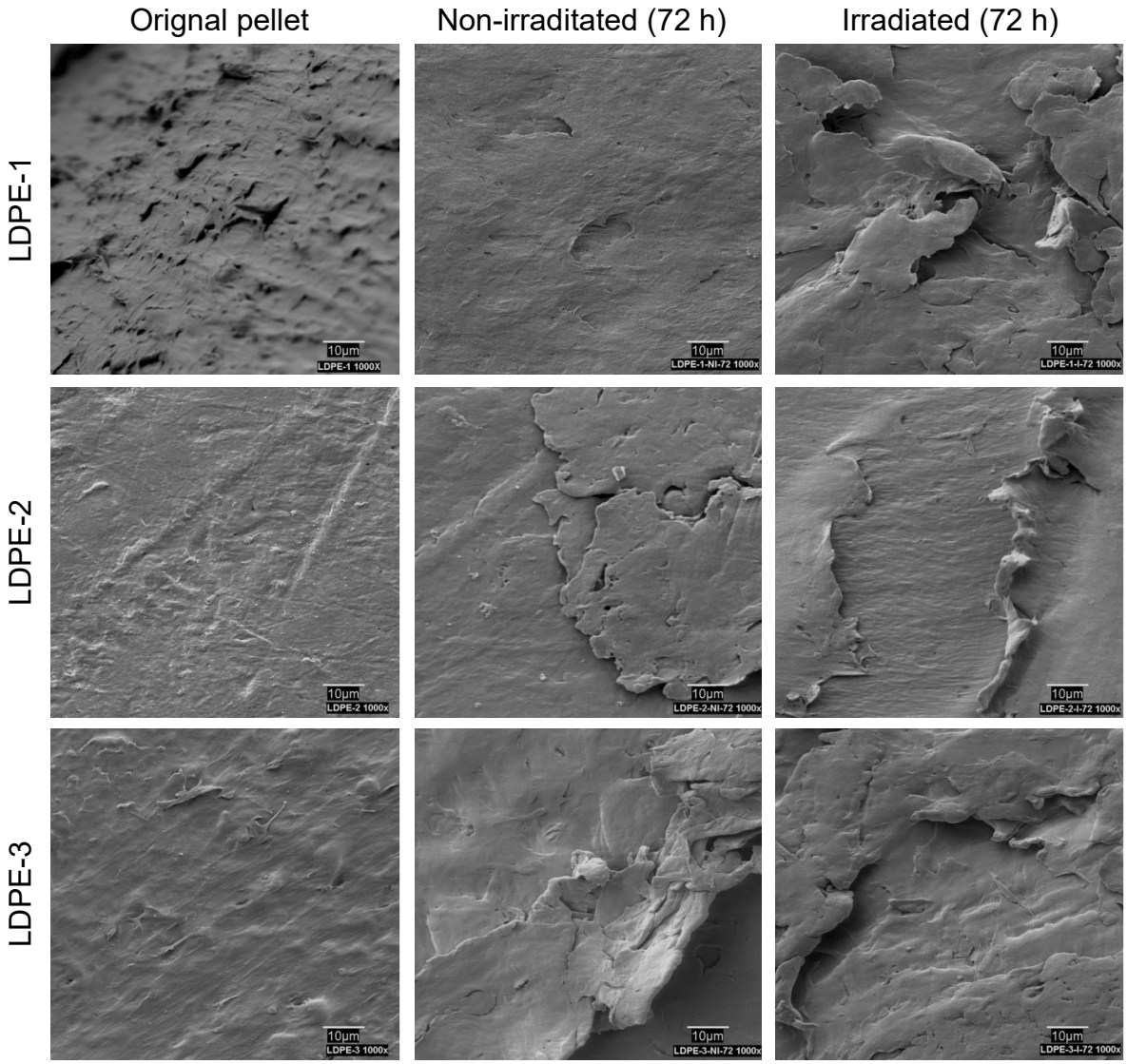

Figure S7. SEM images of the surface of pellets before treatment and after 72 h in irradiated and non-irradiated runs.

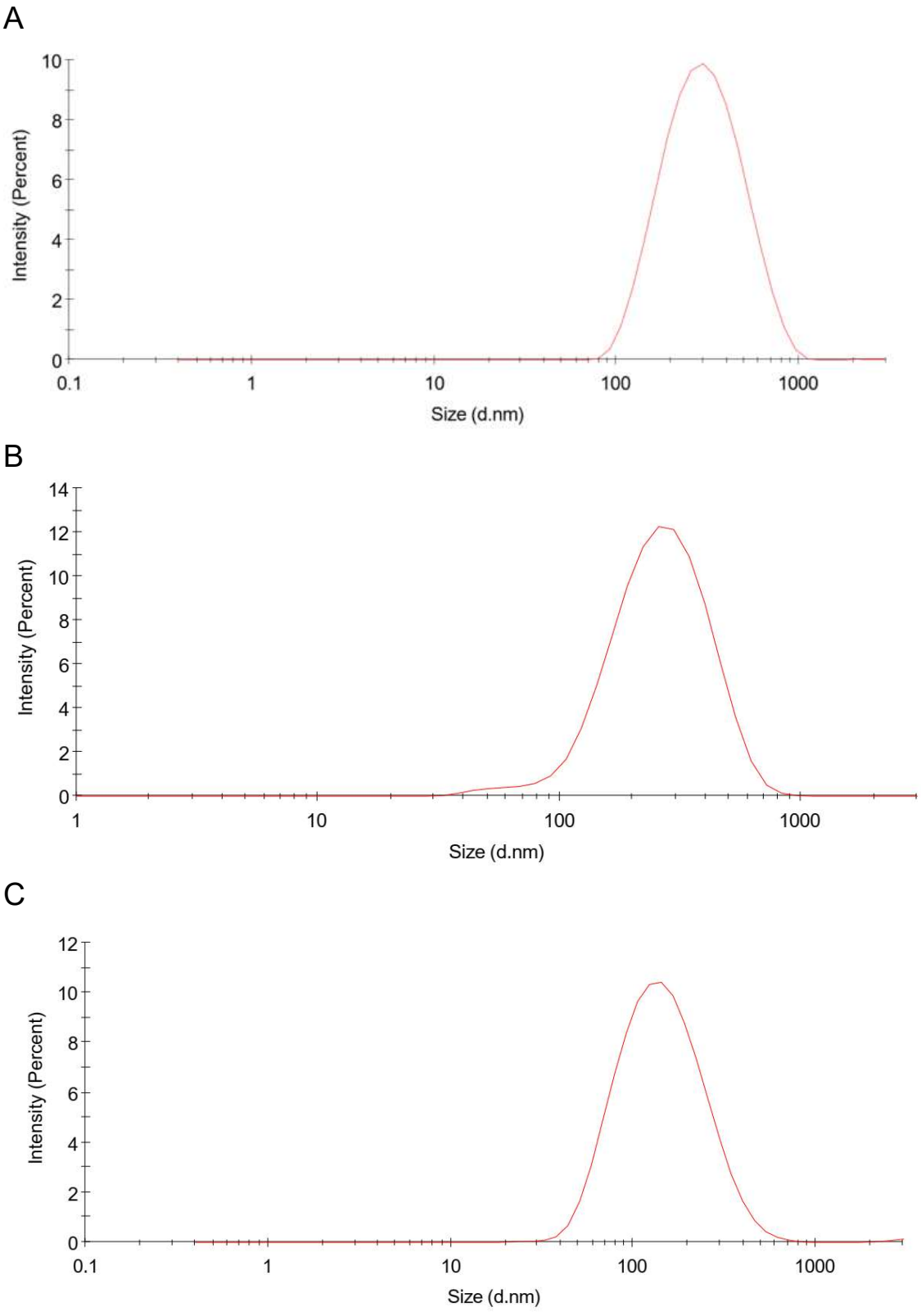

Figure S8. DLS plot for samples LDPE-1-[72]-I (A), LDPE-2-[72]-I (B), and LDPE-3-[72]-I (C).